Title: PREDICTION OF PRIMARY SOMATOSENSORY NEURON ACTIVITY DURING ACTIVE TACTILE EXPLORATION

Authors: Dario Campagner[1], Mathew Evans[1], Michael R. Bale[1,2], Andrew Erskine[1,3], Rasmus S. Petersen[1]

Authors' affiliation: 1. Faculty of Life Sciences, University of Manchester, Stopford Building, Oxford Road, Manchester M13 9PT, UK. 2. School of Life Sciences, University of Sussex, Brighton, BN1 9QG, UK 3. The Francis Crick Institute, Mill Hill Laboratory, The Ridgeway, Mill Hill, London, NW7 1AA.

Correspondence to: r.petersen@manchester.ac.uk

ABSTRACT

Primary sensory neurons form the interface between world and brain. Their function is well-understood during passive stimulation but, under natural behaving conditions, sense organs are under active, motor control. In an attempt to predict primary neuron firing under natural conditions of sensorimotor integration, we recorded from primary mechanosensory neurons of awake, head-fixed mice as they explored a pole with their whiskers, and simultaneously measured both whisker motion and forces with high-speed videography. Using Generalised Linear Models, we found that primary neuron responses were poorly predicted by whisker angle, but well-predicted by rotational forces acting on the whisker: both during touch and free-air whisker motion. These results are in apparent contrast to previous studies of passive stimulation, but could be reconciled by differences in the kinematics-force relationship between active and passive conditions. Thus, simple statistical models can predict rich neural activity elicited by natural, exploratory behaviour involving active movement of the sense organs.

INTRODUCTION

A major challenge of sensory neuroscience is to understand the encoding properties of neurons to the point that their spiking activity can be predicted in the awake animal, during natural behaviour. However, accurate prediction is difficult without experimental control of stimulus parameters and, despite early studies of awake, behaving animals (Hubel, 1959), subsequent work has most often effected experimental control by employing anaesthesia and/or passive stimulation. However, the active character of sensation (Gibson, 1962; Yarbus 1967), based on motor control of the sense organs, is lost in reduced preparations. Recent methodological advances permit a way forward: in the whisker system, it is now possible to record neuronal activity from an awake mouse, actively exploring the environment with its whiskers, whilst simultaneously measuring the fundamental sensory variables (whisker kinematics and mechanics) likely to influence neuronal activity (O'Connor et al. 2010).

Our aim here was to predict spikes fired by primary whisker neurons (PWNs) of awake mice engaged in natural, object exploration behaviour. The manner in which primary neurons encode sensory information fundamentally constrains all downstream neural processing (Lettvin et al. 1959). PWNs innervate mechanoreceptors located in the whisker follicles (Zucker and Welker 1969; Rice et al. 1986). They are both functionally and morphologically diverse; including types responsive to whisker-object contact and/or whisker self-motion (Szwed et al. 2003; Ebara et al. 2002). PWNs project to the cerebral cortex, analogously to other modalities, via trisynaptic pathways through the brainstem and thalamus (Diamond et al. 2008).

Here, we show that PWN responses are well-predicted by rotational force ('moment') acting on the whisker, while whisker angle is a poor predictor. Moment coding accounts for a substantial amount of spiking during both whisker-object interaction and whisker motion in

air. Moment coding can also account for findings in previous studies of passive stimulation in the anaesthetized animal; indicating that the same biomechanical framework can account for primary somatosensory neurons responses across diverse states. Our results provide a mechanical basis for linking receptor mechanisms to tactile behaviour.

RESULTS:

Primary whisker neuron activity during object exploration is predicted by whisker bending moment

We recorded the activity of single PWNs from awake mice (Figure 1A, E, Figure 1-figure supplement 1) as they actively explored a metal pole with their whiskers (N = 20 units). At the same time, we recorded whisker motion and whisker shape using high-speed videography (1000 frames/s; Figure1D, Video 1). As detailed below, PWNs were diverse, with some responding only to touch, others also to whisker motion. Since each PWN innervates a single whisker follicle, we tracked the 'principal whisker' of each recorded unit from frame to frame, and extracted both the angle and curvature of the principal whisker in each video frame (total 1,496,033 frames; Figure1B-E; Bale et al. 2015). Whiskers are intrinsically curved, and the bending moment on a whisker is proportional to how much this curvature changes due to object contact (Birdwell et al. 2007): we therefore used 'curvature change' as a proxy for bending moment (O'Connor et al. 2010a). Whisker-pole contacts caused substantial whisker bending (curvature change), partially correlated with the whisker angle (Figures 1E, 4E) and, consistent with Szwed et al. (2003) and Leiser and Moxon (2007), robust spiking (Figures 1E, 2E).

To test between candidate encoding variables, our strategy was to determine how accurately it was possible to predict PWN activity from either the angular position or curvature change of each recorded unit's principal whisker. To predict spikes from whisker state, we used

Generalised Linear Models (GLMs; Figure 2A). GLMs, driven by whisker angle, have previously been shown to provide a simple but accurate description of the response of PWNs to passive stimulation (Bale et al. 2013) and have mathematical properties ideal for robust parameter-fitting (Truccolo et al. 2005; Paninski et al. 2007).

For each recorded unit (median 69,672 frames and 550 spikes per unit), we computed the GLM parameters that best predicted the unit's spike train given the whisker angle time series using half the data as a training set for parameter-fitting; 8 total fitted parameters - 5 for stimulus filter, 2 for history filter, 1 bias; Figure 2-figure supplement 3). We then assessed prediction performance using the other half of the data as a testing set: we provided the GLM with the whisker angle time series as input and calculated the predicted spike train, evoked in response (Material and Methods). We then compared the recorded spike train to the GLM-predicted one (Figure 2B-C) and quantified the similarity between the smoothed spike trains using the Pearson correlation coefficient (PCC). This is a stringent, single-trial measure of model prediction performance (Figure 2-figure supplement 1B). We then repeated this entire procedure for the whisker curvature time series. Although angle GLMs predicted spike trains of a few units moderately well (2/20 units had PCC > 0.5), they performed poorly for the majority (median PCC 0.06, IQR 0.019-0.3; Figure 2B-D, orange). This was unlikely to be because of non-linear tuning to whisker angle, since quadratic GLMs fared only marginally better (median PCC 0.097, IQR 0.042-0.31; p=0.044, signed-rank test, Figure 2-figure supplement 1A). In contrast, we found that, at the population level, the curvature GLMs were substantially more accurate than the angle GLMs (median PCC 0.52, IQR 0.22-0.66; p=0.0044, signed-rank test; Figure 2B-D, blue) with prediction accuracy up to PCC 0.88. Curvature GLMs also predicted spikes during touch episodes significantly more accurately (median PCC 0.57, IQR 0.23-0.72) than did angle GLMs during non-touch episodes (median 0.06, IQR 0.02-0.35; p=0.005, signed-rank test). At the level of individual units, 90% had

above chance PCC and we termed these ‘curvature-sensitive’ (Material and Methods). Of the curvature-sensitive units, 61% were sensitive to positive curvature change and 39% to negative curvature change (Material and Methods).

The result that curvature predicted PWN responses better than angle was robust to the number of fitted parameters: a GLM sensitive to instantaneous curvature (4 parameters: 1 stimulus filter parameter, 2 history filter parameters and 1 bias) exhibited very similar prediction accuracy (Figure 2-figure supplement 1C). The result was also robust to time-scale: prediction accuracy based on curvature was significantly greater than that based on angle for smoothing time-scales in the range 1-100ms (signed-rank test, $p<0.05$, Bonferroni-corrected).

Although the activity of most units was better predicted by whisker curvature change than by whisker angle, there was significant variability in prediction performance, and there were a few units for which the angle prediction performance was appreciable (Figure 2D). However, we found that this could largely be attributed to redundancy. When a mouse whisks against an object, curvature change and angle fluctuate in concert (Birdwell et al. 2007; Bagdasarian et al. 2013; Pammer et al. 2013; Figures 1E, 4E and Figure 4F-G). When we fitted GLMs using both curvature change and angle as input, these GLMs predicted the spike trains no more accurately (median PCC 0.53 IQR 0.40-0.62; $p=0.067$, signed-rank test; Figure 2D) than GLMs based on curvature change alone. Moreover, on a unit-by-unit basis, for 65% of units, curvature change GLMs predicted spikes better than angle (signed-rank test, $p<0.05$, Bonferroni corrected); only for 5% of units did angle predict spikes better than curvature change. GLMs based on curvature change also predicted spike trains more accurately than GLMs based on “push angle” – the change in angle as the whisker pushes against an object (Figure 1E; median PCC 0.25 IQR 0.04-0.45; $p=0.006$, signed-rank test). Moreover, prediction accuracy of GLMs fitted with both push angle and curvature change (median PCC

126 0.52, IQR 0.2-0.69) inputs was no better than that of GLMs fitted with curvature alone (p =
127 0.43, signed-rank test)

128 In principle, neurons might also be sensitive to the axial force component (parallel to the
129 whisker follicle) and/or lateral force component (orthogonal to axial) associated with
130 whisker-object contact (Figure 1B-C, Figure 1-figure supplement 3; Solomon and Hartmann,
131 2006; Pammer et al. 2013). We restricted our analysis to bending moment since, under our
132 experimental conditions, axial/lateral force components were near-perfectly correlated with
133 bending moment (Figure 2-figure supplement 2) and bending moment is likely to have a
134 major influence on stresses in the follicle (Pammer et al.2013).

135 To further test the curvature-encoding concept, we asked whether curvature GLMs could
136 account for the response of PWNs to whisker-pole touch. To this end, we parsed the video
137 data into episodes of 'touch' and 'non-touch'. Units fired at a higher rate during touch than
138 otherwise (Szwed et al. 2003; Leiser and Moxon, 2007). Without any further parameter-
139 adjustment, the curvature-based GLMs reproduced this effect (Figure 2E): the correlation
140 coefficient between recorded and GLM-predicted firing rate for touch episodes was 0.97.
141 Collectively, the above results indicate that, during active touch, the best predictor of whisker
142 primary afferent firing is not whisker angle but rather the bending moment.

143

144 **Primary whisker neuronal activity during whisking is predicted by moment**

145 During free whisking - in the absence of whisker-pole contact - whisker curvature, and
146 therefore bending moment, changed little (Figure 1E, Figure 4F); consistent with previous
147 studies (Knutsen et al. 2008; Quist et al. 2014). Yet, 50% of recorded units ('whisking-
148 sensitive units') were significantly modulated by whisking amplitude (Figure 3A). Consistent

149 with Szwed et al. (2003), PWNs were diverse: 45% were curvature-sensitive (significant PCC
150 for curvature based GLM); 45% were both whisking and curvature sensitive and 5% were
151 whisking sensitive but not curvature-sensitive.

152 The presence of whisking sensitivity suggests that moment due to whisker bending is not the
153 only force that influences PWN activity. A likely candidate is the moment associated with the
154 rotational acceleration of a whisker: this moment is proportional to the whisker's angular
155 acceleration (Quist et al. 2014; Material and Methods). Consistent with this possibility, we
156 found that whisking-sensitive units were tuned to angular acceleration (Figure 3B) and that
157 50% of these were phase-modulated (Figure 3C). Angular acceleration tuning was diverse:
158 some units fired to acceleration in a particular direction (rostral or caudal), whilst others
159 responded to acceleration in both directions (Figure 3B, Figure 3-figure supplement 1).
160 Moreover, for whisking-sensitive units (but not whisking-insensitive ones), quadratic GLMs
161 trained on data from non-touch episodes were able to predict spikes using whisker angle
162 acceleration as input (Figure 3D-E; whisking sensitive units, median PCC 0.37, IQR 0.18-
163 0.58; non-whisking sensitive, median PCC -0.0071, IQR -0.035-0.041; p=0.0017 rank-sum
164 test for whisking-sensitive vs non whisking-sensitive units). For 70% of whisking-sensitive
165 units, directional selectivity for acceleration was consistent with that for curvature. These
166 findings indicate that, in the absence of whisker-object contact, responses of PWNs to
167 whisking itself can be accounted for by sensitivity to the moment associated with angular
168 whisker acceleration.

169

170 **Relation between kinematics and mechanics is different in active vs passive touch and**
171 **has implications for neural encoding**

We found, during active object exploration, that curvature change, but not whisker angle, predicts PWN firing. In apparent contrast, studies using passive whisker stimulation have reported that PWNs encode whisker angle and its temporal derivatives (Zucker and Welker, 1969; Gibson and Welker, 1983; Lichtenstein et al. 1990; Jones et al. 2004; Arabzadeh et al. 2005; Bale and Petersen, 2009; Lottem and Azouz, 2011; Bale et al. 2013). We wondered whether the discrepancy might be due to differences in whisker mechanics between passive and active stimulation conditions. To test this, we analysed the relationship between angle and curvature change during active touch and compared it to that during passive whisker stimulation. During active pole exploration, angle and curvature change were, over all, only loosely related (median correlation coefficient 0.20, IQR 0.079-0.39, Figures 4D-E). Important contributory factors were that the angle-curvature relationship was both different for touch compared to non-touch (Figure 4F) and dependent on object location (Figure 4G).In contrast, during passive stimulation, whisker angle was near perfectly correlated with curvature change (for C2, correlation coefficients 0.96 and 0.94 respectively; similar results for C5; Figures 4C-D, Figure 4E, inset and Figure 4-figure supplement 2); consistent with properties of cantilevered beams (Birdwell et al. 2007). Simulations confirmed that, due to the tight relationship between the variables, a unit tuned only to curvature change can appear tightly tuned to angle (Figure 4-figure supplement 1). The implication is that apparent sensitivity to whisker angle under passive stimulation conditions can be accounted for by moment-tuning.

DISCUSSION

Prediction of spikes fired by sensory neurons under natural conditions

In the endeavour to understand how neurons encode and process sensory information, there is a basic tension between the desire for tight experimental control and the desire to study animals under natural, unconstrained conditions. Theories of sensory encoding suggest that neural circuits have evolved to operate efficiently under natural conditions (Simoncelli and Olshausen, 2001; Reinagel 2001). Previous studies have succeeded in predicting/decoding spikes evoked by passive presentation of natural sensory stimuli to anaesthetised/immobilised animals (Lewen et al. 2001; Arabzadeh et al. 2005; Pillow et al. 2008; Mante et al. 2008; Lottem and Azouz, 2011; Bale et al. 2013), but it has been difficult to extend this approach to encompass natural, active movement of the sense organs. Here we have addressed this general issue, taking advantage of experimental possibilities recently created in the whisker system (O'Connor et al.2010a), and the ability of computational methods, such as GLMs, to uncover stimulus-response relationships even from data with complex statistical structure (Paninski et al. 2007; Fairhall and Sompolinski, 2014). Our main finding was that responses of PWNs, recorded as an awake mouse actively explores an object with its whiskers, can be predicted from the forces acting on the whiskers. Given that, for each unit, we were attempting to predict the entire ~70 s time course of activity, the variability of the behaviour of untrained mice (O'Connor et al. 2010a), and the lack of trial-averaging as a noise reduction strategy, it is remarkable that we found model prediction correlation coefficients up to 0.88. A challenge of studying neural coding under unconstrained, awake conditions is that sensory variables tend to correlate. A useful feature of the GLM training procedure is that it takes such correlations into account. We found that, although whisker angle predicted spikes for a subset of units, this effect was very largely explained by a curvature-coding model, together with the correlation between angle and curvature.

Mechanical framework for tactile coding

Pushing a whisker against an object triggers spiking in many PWNs (Szwed et al. 2003, 2006; Leiser and Moxon, 2007). Biomechanical modelling by Hartmann and co-workers accounts for this by a framework where the whisker is idealised as an elastic beam, cantilever-mounted in the skin (Birdwell et al. 2007; Quist et al. 2014). When such a beam pushes against an object, the beam bends, causing reaction forces at its base. Our data are in striking agreement with the general suggestion that mechanoreceptor activity is closely related to such reaction forces. Our results show that curvature change associated both with contact-induced whisker bending and with whisker rotation predicts PWN spiking. Our results also provide a mechanical basis for previous findings: our finding of subtypes of curvature-only and curvature-acceleration PWNs is consistent with previous reports of 'touch' and 'whisking-touch' units (Szwed et al. 2003; 2006). Thus, a common framework accounts for diverse PWN properties.

Our finding that whisker angle predicts PWN spikes poorly indicates that whisker angle can change without modulating mechanotransduction in the follicle. This is consistent with evidence that, during artificial whisking, the follicle-shaft complex moves as a rigid unit (Bagdasarian et al. 2013). In apparent contrast, previous studies using passive stimulation in anaesthetised animals have consistently reported a tight relationship between whisker kinematics and PWN response. In the cantilever whisker model, passively induced changes in whisker angle correlate highly with whisker bending. We confirmed that this applies to real whiskers *in vivo* and demonstrate that moment-sensitive units can thereby appear angle-tuned. In this way, moment-encoding can account for primary neuron responses not only during active touch but also under passive stimulation. More generally, our results highlight the importance of studying neurons under natural, active sensing conditions.

In this study, we considered PWN encoding under conditions of pole contact, since this is well-suited to reaction force estimation (O'Connor et al. 2010a; Pammer et al. 2013) and

involves object-stimulus interactions on a ~100 ms time-scale that is conducive to single-trial analysis. Since whisker bending is ubiquitous in whisking behaviour, it is likely that our finding of curvature sensitivity is a general one. However, prediction performance varied across units, suggesting that other force components may also be encoded. Other experimental conditions – for example, textured surfaces – may involve multiple force components (Quist and Hartmann 2012; Pammer et al. 2013; Bagdasarian et al. 2013) and/or encoding of information by spike timing on a finer time-scale (Panzeri et al. 2001; Petersen et al. 2001; Arabzadeh et al. 2005; Bale et al. 2015).

It is axiomatic that mechanoreceptors are sensors of internal forces acting in the tissue within which they are embedded (Abraira and Ginty, 2013) and therefore valuable to be able to measure mechanical forces in the awake, behaving animal. In general, including the important case of primate hand-use, the complex biomechanics of skin makes force-estimation difficult (Phillips and Johnson, 1981). In contrast, for whiskers, the quasi-static relationship is relatively simple: the bending moment on a whisker is proportional to its curvature and this has the important implication that reaction forces can be directly estimated from videography *in vivo* (Birdwell et al. 2007; O'Connor et al. 2010a; Pammer et al. 2013). Our results are the first direct demonstration that such reaction forces drive primary sensory neuron responses – likely involving Piezo2 ion channels (Woo et al. 2014; Poole et al. 2015;Whiteley et al. 2015) – and provide insight into how sensitivity to touch and self-motion arises in the somatosensory pathway (Szwed et al. 2003; Yu et al. 2006; Curtis and Kleinfeld, 2009; O'Connor et al. 2010b; Curtis and Kleinfeld, 2009; Huber et al. 2012; Petreanu et al. 2012; Peron et al. 2015).

Moment-based computations in tactile behaviour

Extraction of bending moment is a useful first step for many tactile computations. Large transients in bending moment signal object-touch events, and the magnitude of bending is inversely proportional to the radial distance of contact along the whisker (Solomon and Hartmann, 2006). As illustrated by our results on the statistics of active touch, if integrated with cues for whisker self-motion, whisker bending can be a cue to the 3D location of an object (Szwed et al. 2003, Szwed et al. 2006, Birdwell et al. 2007; Bagdasarian et al. 2013; Pammer et al. 2013). Bending moment can permit wall following (Sofroniew et al. 2014) and, if integrated across whiskers, can in principle be used both to infer object shape (Solomon and Hartmann, 2006) and to map the spatial structure of the environment (Fox et al. 2012, Pearson et al. 2013).

Summary and Conclusion

We have shown that the responses of primary whisker neurons can be predicted, during natural behaviour that includes active motor control of the sense organ, from forces acting on the whiskers. These results provide a bridge linking receptor mechanisms to behaviour.

MATERIAL AND METHODS

All experimental protocols were approved by both United Kingdom Home Office national authorities and institutional ethical review.

Surgical procedure

Mice (C57; N=10; 6 weeks at time of implant) were anesthetized with isoflurane (2% by volume in O_2), mounted in a stereotaxic apparatus (Narishige) and body temperature maintained at 37°C using a homeothermic heating system. The skull was exposed and a titanium head-bar (19.1mm x 3.2mm x 1.3mm; O'Connor et al. 2010a) was first attached to the skull ~1 mm posterior to lambda (Vetbond), and then fixed in place with dental acrylic (Lang dental). A craniotomy was made (+0.5mm to -1.5mm posterior to bregma, 0mm to 3mm lateral) and sealed with silicone elastomer. Buprenorphine (0.1 mg/kg) was injected subcutaneously for postoperative analgesia and the mouse left to recover for at least 5 days

Behavioural apparatus

Mice were studied in a pole exploration apparatus adapted from O'Connor et al. (2010a) but were not trained on any task. A mouse was placed inside a perspex tube (inner diameter 32 mm), from which its head emerged at one end, and immobilised by fixing the head-bar to a custom mount holder. The whiskers were free of the tube at all times. The stimulus object was a 1.59 mm diameter metal pole, located ~3.5mm lateral to the mouse's snout. To allow control of its anterior/posterior location, the pole was mounted on a frictionless linear slide (Schneeberger NDN 2-50.40) and coupled to a linear stepper motor (Zaber NA08B30). To allow vertical movement of the pole into and out of range of the whiskers, the pole/actuator assembly was mounted on a pneumatic linear slide (Festo SLS-10-30-P-A), powered by compressed air. The airflow was controlled by a relay (Weidmüller). In this way, the pole

307 moved rapidly (~0.15 s) into and out of range of the whiskers. The apparatus was controlled
308 from Matlab via a real-time processor (TDT, RX8).

309 **Electrophysiology**

310 We recorded the activity of PWNs from awake mice in the following way. To permit reliable
311 whisker tracking (see below), before each recording session, A, B and E whisker rows were
312 trimmed to the level of the fur, under brief isoflurane anaesthesia. The trigeminal ganglion
313 was targeted as previously described (Bale et al. 2015). The silicone seal was removed and a
314 3/4 shank tungsten microelectrode array (FHC, recording electrodes 8MΩ at 1kHz, reference
315 1MΩ; tip spacing ~500 μm) was lowered through the brain (angle 4 ° to vertical in the
316 coronal plane) using a micromanipulator (Scientifica, PatchStar) under isoflurane
317 anaesthesia. Extracellular potentials were pre-amplified, digitised (24.4 kHz), filtered (band
318 pass 300-3000 Hz) and acquired continuously to hard disk (TDT, RZ5). The trigeminal
319 ganglion was encountered 6-7 mm vertically below the pial surface and whisker-response
320 units identified by manual deflection of the whiskers with a small probe. Once a well-isolated
321 unit was found, the whisker that it innervated (the 'principal whisker', PW) was identified by
322 manual stimulation. To define the PW, we deflected not only untrimmed whiskers but also
323 the stubs of the trimmed whiskers. Any unit whose PW was a trimmed whisker was ignored.
324 At this point, anaesthesia was discontinued. Once the mouse was awake, we recorded
325 neuronal activity during repeated presentations of the pole ('trials'). Before the start of each
326 trial, the pole was in the down position, out of reach of the whiskers. The pole was first
327 moved anterior-posteriorly to a position chosen randomly out of a set of 11 possible
328 positions, spanning a range ±6 mm with respect to the resting position of the base of the PW.
329 A trial was initiated by activating the pneumatic slide relay, thus moving the pole up into the
330 whisker field, where it remained for 3s before being lowered. At the end of a recording

331 session, the microelectrode array was withdrawn, the craniotomy sealed with silicone
332 elastomer, and the mouse returned to its home cage.

333 **High-speed videography**

334 Using the method of O'Connor et al. (2010a) to image whisker movement/shape, whiskers
335 ipsilateral to the recorded ganglion were illuminated from below using a high-power infrared
336 LED array (940 nm; Roithner, LED 940-66-60) via a diffuser and condensing lens. The
337 whiskers were imaged through a telecentric lens (Edmunds Optics, 55-349) mounted on a
338 high speed camera (Mikrotron, LTR2; 1000 frames/s, 0.4 ms exposure time). The field of
339 view of the whiskers was 350x350 pixels, with pixel width 0.057mm.

340 **Response to touch and non-touch events**

341 Mouse whisking behaviour during the awake recording was segmented into 'touch', and 'non-
342 touch' episodes. Touches between the PW of each unit and the pole were detected manually
343 in each frame of the high-speed video. A frame was scored as touch if no background pixels
344 were visible between the pole silhouette and the whisker. Any frame not scored as a touch
345 was scored as non-touch. Touch and non-touch firing rates for a given unit were computed by
346 averaging activity over all corresponding episodes.

347 **Whisker tracking**

348 Since the trigeminal ganglion lacks topography, it is difficult to target units that innervate a
349 specific whisker, and therefore desirable for a whisker tracker to be robust to the presence of
350 multiple rows of whiskers. However, since neurons in the ganglion innervate individual
351 whiskers, it is sufficient to track only one whisker (the PW) for each recorded neuron. To
352 extract kinematic/mechanical whisker information, we therefore developed a whisker tracker
353 ('WhiskerMan'; Bale et al. 2015) whose design criteria, different to those of other trackers
354 (Perkon et al. 2011; Clack et al. 2012), were to: (1) be robust to whisker cross-over events;

(2) track a single, target whisker; (3) track the proximal segment of the whisker shaft. The shape of the target whisker segment was described by a quadratic Bezier curve $\mathbf{r}(t,s)$ (a good approximation away from the zone of whisker-object contact; Quist and Hartmann, 2012; Pammer et al. 2013): $\mathbf{r}(t,s) = [x(t,s), y(t,s)]$, where x, y are horizontal/vertical coordinates of the image, $s = [0,..,1]$ parameterises (x,y) location along the curve and t is time. We fitted such a Bezier curve to the target whisker in each image frame using a local, gradient-based search. The initial conditions for the search were determined by extrapolating the solution curves from the previous two frames, assuming locally constant, angular velocity. The combination of the low-parameter whisker description and the targeted, local search makes the algorithm robust to whisker cross-over events. The 'base' of the target whisker was defined as the intersection between the extrapolated Bezier curve and the snout contour (estimated as described in Bale et al. 2015). The solution curve in each frame was visually checked and the curves manually adjusted to correct occasional errors.

Estimation of kinematic/force parameters

The whisker angle (θ) in each frame was measured as the angle between the tangent to the whisker curve at the base and the anterior-posterior axis (Figure 1B). Whisker curvature (κ) was measured at the base as $\kappa = \frac{x'y''-x''y'}{(x'^2+y'^2)^{3/2}}$, where x', y' and x'', y'' are the first and second partial derivatives of the functions $x(s)$ and $y(s)$ with respect to s (Figure 1B). Since reaction force at the whisker base reflects changes in whisker curvature, rather than the intrinsic (unforced) curvature (Birdwell et al. 2007), we computed 'curvature change' $\Delta\kappa = \kappa - \kappa_{int}$, where κ_{int}, the intrinsic curvature, was estimated as the average of κ in the first 100 ms of the trial (before pole contact; O'Connor et al. 2010a). During free whisking, whisker angle oscillated with the characteristic whisking rhythm, but curvature changed little. The small changes in whisker curvature during free whisking were consistent with torsional effects

379 (Knutsen et al. 2008). We estimated the number of whisking cycles from the duration of
380 touch/non-touch episodes and the whisking frequency: median 419 whisking cycles per unit
381 during touch periods; 415 during non-touch periods.

382 Under conditions of whisking against a smooth surface, such as in the present study, the
383 quasi-static framework of Birdwell et al. (2007) applies. Δκ, measured, at the base of a
384 whisker, in horizontal given plane, is proportional to the component of bending moment in
385 that plane. We used Δκ as a proxy for bending moment. Bending moment (M), Axial ($\vec{F}_{ax}$)
386 and lateral forces ($\vec{F}_{lat}$) at the whisker base were calculated, during periods of whisker-pole
387 contact, using the method of Pammer et al. (2013), using published data on areal moment of
388 inertia of mouse whiskers (Quist and Hartmann, 2012), along with whisker-pole contact
389 location (see figure 1-figure supplement 3 for details). Pole location, in the horizontal plane,
390 in each frame, was identified as the peak of a 2D convolution between the video image and a
391 circular pole template. To localise whisker-pole contact, the whisker tracker was used to fit
392 the distal segment of the whisker close to the pole, seeded by extrapolation from the whisker
393 tracking solution for the proximal whisker segment, described above. Whisker-pole contact
394 location was defined as the point where this distal curve segment was closest to the detected
395 pole centre. Pole and contact locations were verified by visual inspection.

396 As expressed by Newton's second law of rotational motion, the moment – or torque – of a
397 rigid body, rotating in a plane, is proportional to the body's angular acceleration. During free
398 whisking, a whisker behaves approximately as a rigid body and, for the whiskers considered
399 in this study, their motion is predominantly in the horizontal plane (Bermejo et al. 2002,
400 Knutsen et al. 2008). Thus, to assess whether such a moment is encoded by PWNs, we
401 measured angular whisker acceleration during free whisking as a proxy. Acceleration was

402 calculated from the whisker angle time series after smoothing with a Savitzky-Golay filter
403 (polynomial order 5; frame size 31 ms).

404 Push angle – the change in angle as a whisker pushes against an object - was measured during
405 touch epochs. For each touch episode, we determined the value of the angle in the frame
406 before touch onset and subtracted this from the whisker angles during the touch.

407 **Passive whisker deflection**

408 To determine how whiskers move/bend in response to passive deflection under anaesthesia, a
409 mouse was anesthetized (isoflurane 2%) and placed in the head-fixation apparatus. Individual
410 whiskers (C2 and C5 trimmed to 5 mm) were mechanically deflected using a piezoelectric
411 actuator as previously described (Bale et al. 2013; Bale et al. 2015). All other whiskers were
412 trimmed to the level of the fur. Each whisker, in turn, was inserted into a snugly fitting plastic
413 tube attached to the actuator, such that the whisker entered the tube 2 mm from the face. Two
414 stimuli were generated via a real-time processor (TDT, RX8): (1) a 10 Hz trapezoidal wave
415 (duration 3 s, amplitude 8°); (2) Gaussian white noise (duration 3 s, smoothed by convolution
416 with a decaying exponential: time constant 10 ms; amplitude SD 2.1 °). During the
417 stimulation, the whiskers were imaged as detailed above (1000 frames/s, 0.2 ms exposure
418 time).

419 **Electrophysiological data analysis**

420 *Spike sorting*: Single units (N=20) were isolated from the extracellular recordings as
421 previously described, by thresholding and clustering in the space of 3-5 principal components
422 using a mixture model (Bale and Petersen, 2009). A putative unit was only accepted if (1) its
423 inter-spike interval histogram exhibited a clear absolute refractory period and (2) its
424 waveform shape was consistent between the anaesthetised and awake phases of the recording.

Responses to whisking without touch: To test whether a unit responded to whisking itself, we extracted non-touch episodes as detailed above and computed time series of whisking amplitude and phase by band-pass filtering the whisker angle time series (6-30Hz) and computing the Hilbert transform (Kleinfeld and Deschênes 2011). Amplitudes were discretised (30 equi-populated bins) and the spiking data used to compute amplitude tuning functions. Phases for bins where the amplitude exceeded a given threshold were discretised (8 equi-populated bins) and used to construct phase tuning functions. To determine whether a unit was significantly amplitude-tuned, we fitted a regression line to its amplitude tuning curve and tested whether the slope was statistically significantly different to 0 (p=0.0025, Bonferroni corrected). To determine whether a unit was significantly phase-tuned, we computed the maximum value of its phase tuning curve and compared this to the distribution of maxima of chance tuning functions. Chance tuning functions were obtained by randomly shifting the recorded spike sequences by 3000-8000 ms and recomputing tuning functions (500 times). A unit was considered phase-tuned if its tuning function maximum (computed using amplitude threshold of 2°) exceeded the 95th percentile of the shuffled distribution.

Acceleration tuning curves were quantified, for each unit, as follows. First, an acceleration tuning curve was estimated (as above). Units typically responded to both positive and negative accelerations, but with unequal weighting between them. To capture this, we fitted the following regression model to the tuning curve:

$$r_i = \mu_0 + \mu_1|a_i| + \mu_2\Delta_i + \mu_3\Delta_i|a_i|$$

Here, for each bin i of the tuning curve, r_i was the firing rate and a_i was the acceleration; μ_0 μ_1, μ_2 and μ_3 were regression coefficients; the term Δ_i (Δ_i=1 if a_i<0, Δ_i=0 otherwise) allowed for asymmetric responses to negative and positive acceleration. Based on its best-fitting regression coefficients (p=0.05), units were classified as: having 'preference for negative

acceleration', if μ_3 was significantly >0; having 'preference for positive acceleration', if μ_3 was significantly <0; as having 'no preferred direction' if both μ_1 was significantly >0, and μ_3 was not significantly >0; and as 'not acceleration sensitive' if neither μ_1 nor μ_3 were significantly >0.

Generalised Linear Model (GLM): To investigate how well PWNs encode a given sensory variable (e.g., whisker angle, curvature), we fitted single unit activity to a GLM (Nelder and Wedderburn, 1972; Truccolo et al. 2005; Paninski et al. 2007), using methods similar to Bale et al. (2013). For each unit, a 'stimulus' time series (x) (whisker angle or whisker curvature change) and a simultaneously recorded spike time series (n) were discretized into 1 ms bins: x_t and n_t denote respectively the stimulus value and spike count (0 or 1) in bin t.

GLMs express how the expected spike count of a unit depends both on the recent stimulus history and on the unit's recent spiking history. The standard functional form of the model we used was:

$$y_t = f\left(\vec{k}^T\overrightarrow{x_t} + \vec{h}^T\overrightarrow{n^*_t} + b\right), \qquad (1)$$

Here n^*_t, the output in bin t, was a Bernoulli (spike or no-spike) random variable. The probability of a spike in bin t, y_t, depended on three terms: (1) the dot product between the stimulus history vector $\overrightarrow{x_t} = (x_{t-Lk+1},\ldots,x_t)$ and a 'stimulus filter' $\vec{k}$ (length $L_k = 5$); (2) the dot product between the spike history vector $\vec{n}^* = (n^*_{t-Lh+1},\ldots,n^*_t)$ and a 'spike history filter' $\vec{h}_t$ (length $L_h = 2$); (3) a constant b, which set the spontaneous firing rate. $f(\cdot)$ was the logistic function $f(z) = (1 + e^{-z})^{-1}$. The preferred direction of the GLM is determined by the sign of the stimulus filter. Positive (negative) k coefficients tend to make positive (negative) stimuli trigger spikes. Since we found that GLM performance was just as good with $L_k = 1$ as $L_k = 5$ (Figure 2-figure supplement 1C), we used results from the $L_k = 1$ case to define

selectivity to curvature change direction: positive k implies selectivity for positive curvature change; negative k selectivity for negative curvature change. When a whisker pushes against an object during protraction, curvature increases; when it pushes against an object during retraction, it decreases.

To consider whether units might encode multiple sensory variables (e.g., both whisker angle and whisker curvature change), we used a GLM with multiple stimulus history terms, one for each sensory variable:

$$y_t = f\left(\vec{k}_1^T \overrightarrow{x_{t;1}} + \vec{k}_2^T \overrightarrow{x_{t;2}} + \vec{h}_t^T \overrightarrow{n^*} + b\right)$$

Here the indices 1, 2 label the sensory variables.

Training and testing of the GLM was done using a cross-validation procedure. For each unit, half of the trials were assigned randomly to a training set and half to a testing set. The training set was used to fit the parameters ($\vec{k}$, $\vec{h}$ and b), while the testing set was used to quantify the similarity between the spike train of the recorded unit and that predicted by the GLM. GLM fitting was achieved by finding the parameter values ($\vec{k}$, $\vec{h}$ and b), which minimized a cost function consisting of the sum of the negative log-likelihood and a regularizing term $-\propto \|\vec{k}\|^2$. For all units, model prediction performance on the test set was robust to variation of α over several orders of magnitude: α was therefore set to a standard value of 0.01. To quantify the performance of the model, the sensory time series of the testing set was used as input to the best-fitting GLM to generate a 'predicted' spike train in response. Both real and predicted spike trains were then smoothed by convolution with a 100 ms box-car filter and the similarity between them quantified by the Pearson correlation coefficient (PCC). For each unit, the entire training/testing procedure was repeated for 10 random choices of training/testing set and the final prediction accuracy defined as the median of the

493 10 resulting PCC values. Data from these 10 samples were also used to test whether an
494 individual unit exhibited statistically significant prediction performance for different sensory
495 features. To test whether the results were robust to the smoothing time-scale, the above
496 procedure was repeated for a range of box-car smoothing filters (1, 5, 10, 20, 50, 70 ms). To
497 test whether a given 'actual' PCC was statistically significant, we tested the null hypothesis
498 that it could be explained by random firing at the same time-averaged rate as that of the
499 recorded unit. To this end, the recorded spike sequences were randomly shifted by 3000-8000
500 ms and the training/testing procedure above applied to this surrogate data. This was repeated
501 10 times and the resulting chance PCCs compared to the actual PCC using a signed-rank test,
502 p=0.0025 (Bonferroni corrected). This analysis was used to classify units as being 'curvature-
503 sensitive'.

504 *Quadratic GLM:* To test whether the units might exhibit nonlinear dependence on the
505 stimulus parameters, we adapted the GLM defined above (equation 1) to include quadratic
506 stimulus variables (Rajan et al. 2013). This was important to assess whisker angular
507 acceleration during free whisking, since a subset of units exhibited U-shaped acceleration
508 tuning functions (Figure 3B). Given a stimulus time series x_t, the quadratic stimulus history
509 vector was $[x_{t-Lk+1},\ldots,x_t,x^2_{t-Lk+1},\ldots,x^2_t]$. Fitting methods were otherwise identical to those
510 detailed above.

511 *Effect of angle-curvature correlations on apparent neuronal stimulus encoding in the passive*
512 *stimulation protocol:* If, in a given recording, sensory variable X correlates with sensory
513 variable Y, a neuron responsive purely to X will tend to appear tuned to Y. To investigate
514 whether such an effect might produce apparent sensitivity to whisker angle in the passive
515 stimulation paradigm, we simulated the response of curvature-tuned neurons to the whisker
516 curvature change time series measured during passive white noise stimulation. To minimise
517 free parameters, constrained GLMs (4 free parameters) were used, sensitive either to

instantaneous curvature ($\vec{k} = [\gamma]$) or to its first order derivative ($\vec{k} = \gamma$ [-1 1]), where γ was a signed, gain parameter. Parameters ($\vec{h}$, b, γ) were adjusted to produce two spike trains (one for training, the other for testing) with a realistic white noise induced firing rate (~50 spikes/s; Bale et al. 2013) . We then attempted to predict the simulated, curvature-evoked (training) spike train by fitting GLMs (length 5 stimulus filter, 8 free parameters) using as input either angle or curvature change. Cross-validated model accuracy was computed as the PCC between the predicted spike train and the testing spike train (both smoothed by convolution with a 5 ms box-car).

Effect of single-trial approach on GLM prediction performance: The objective of encoding models, such as GLMs, is to obtain an accurate description of the mapping between a stimulus and the neuronal spike trains it evokes. Since the random component of a neuron's response is inherently unpredictable, the best any model can do is to predict the probability of the spike train. To enable this, encoding models have generally (with few exceptions; Park et al. 2014) been applied to a 'repeated-trials' paradigm, where a stimulus sequence (e.g., frozen white noise) is repeated on multiple 'trials' (Arabzadeh et al. 2005; Lottem and Azouz, 2011; Bale et al. 2013; Petersen et al. 2008; Pillow et al. 2008). Model accuracy can then be quantified, largely free of contamination from random response variability, by comparing (using PCC or otherwise) the trial-averaged response of the model to the trial-averaged response of the neuron.

In contrast, in the present study of awake, actively whisking mice, the precise stimulus (time series of whisker angle/curvature) was inevitably different on every pole presentation: there were no precisely repeated trials to average over. Our standard model performance metric (PCC) was computed by comparing the response on a single long, concatenated 'trial' the

corresponding GLM predicted response. Such a PCC is downwards biased by random response variability.

To gauge the approximate magnitude of this downward bias, we used a simulation approach. By simulating the response of model neurons, we could deliver identical, repeated trials and, thereby compare model prediction performance by a metric based on trial-averaging with that based on the single-trial approach. To this end, for each recorded unit, we used the best-fitting curvature change GLM to generate 100 trials of spike trains evoked by the curvature time series measured for that unit. Data from the first of these trials was used to fit the parameters of a minimal 'refitted GLM' (stimulus filter length 1, spike history filter length 2; bias; total 4 free parameters), and the single-trial performance quantified, using the approach of the main text (Figure 2-figure supplement 1B, left). Next, we used the refitted GLM to generate 100 repeated trials of spike trains evoked by the curvature time series. Repeated-trials performance was then quantified as the PCC between PSTHs obtained by trial-averaging (Figure 2, -figure supplement 1B, right).

ACKNOWLEDGEMENTS:

We thank S. Fox, M. Humphries, M. Loft, R. Lucas, M. Montemurro and M. Maravall for comments on the manuscript/discussion; K. Svoboda for sharing behavioural methods; G. Caspani, K. Chlebikova, B. Nathanson and R. Twaites for assistance with whisker tracking.

AUTHOR CONTRIBUTIONS:

DC and RSP designed the study. DC and AE performed the experiments. DC, MHE and RSP analyzed the data.MRB, AE, DC and RSP developed the experimental methods. DC, MHE and RSP wrote the manuscript, with input from all authors.

CONFLICT OF INTERESTS:

The authors declare no competing financial interests.

REFERENCES

Abraira VE and Ginty DD. 2013. The sensory neurons of touch. *Neuron,* **79**: 618-639. doi:10.1016/j.neuron.2013.07.051

Arabzadeh E, Zorzin E and Diamond ME. 2005. Neuronal encoding of texture in the whisker sensory pathway. *PLoSBiol,* **3**:e17.doi: 10.1371/journal.pbio.0030017

Bagdasarian K, Swed M., Knutsen PM, Deutsch D, Derdikman D, Pietr M, Simony E. and Ahissar E. 2013. Pre-neuronal morphological processing of object location by individual whiskers. *Nat Neurosci*, **16**:622-631. doi:10.1038/nn.3378

Bale MR and Petersen RS. 2009. Transformation in the neural code for whisker deflection direction along the lemniscal pathway. *J Neurophysiol,* **102**:2771-2780. doi: 10.1152/jn.00636.2009

Bale MR, Campagner D, Erskine A and Petersen RS. 2015. Microsecond-Scale Timing Precision in Rodent Trigeminal Primary Afferents, *J Neurosci,* **35**: 5935-5940. doi: 10.1523/JNEUROSCI.3876-14.2015

Bale MR, Davies K, Freeman OJ, Ince RA and Petersen RS. 2013. Low-dimensional sensory feature representation by trigeminal primary afferents. *J Neurosci,* **33**: 12003-12012. doi: 10.1523/JNEUROSCI.0925-13.2013

Bermejo R, Vyas A, and Zeigler HP. 2002. Topography of rodent whisking-I. Two-dimensional monitoring of whisker movements. *Somatosens Mot Res*, **19(4)**: 341-346.doi: 10.1080/0899022021000037809

Birdwell JA, Solomon JH, Thajchayapong M, Taylor, MA, Cheely M, Towal RB, Conradt J and Hartmann MJZ. 2007. Biomechanical models for radial distance determination by the rat vibrissal system. *J Neurophysiol,* **98**:2439–2455. doi: 10.1152/jn.00707.2006

Clack NG, O'Connor DH, Huber D, Petreanu L, Hires A, Peron S, Svoboda K, Myers EW. 2012. Automated tracking of whiskers in videos of head fixed rodents. *PloS Comput Biol,* **8**:e1002591. doi: 10.1371/journal.pcbi.1002591

Curtis JC and Kleinfeld D. 2009. Phase-to-rate transformations encode touch in cortical neurons of a scanning sensorimotor system. *Nat Neurosci,* **12(4)**: 492-501.doi:10.1038/nn.2283

Diamond ME, von Heimendahl M, Knutsen PM, Kleinfeld D and Ahissar E. 2008. 'Where' and 'what' in the whisker sensorimotor system. *Nat Rev Neurosci*, **9(8)**: 601-612. doi:10.1038/nrn2411

Ebara S, Kumamoto K, Matsuura T, Mazurkiewicz JE and Rice FL. 2002. Similarities and differences in the innervation of mystacial vibrissal follicle–sinus complexes in the rat and cat: a confocal microscopic study. *J Comp Neurol*, **449(2)**, 103-119. doi: 10.1002/cne.10277

Fairhall A and Sompolisky H. 2014. Editorial overview: theoretical and computational neuroscience. *Curr Opin Neurobiol,* **25**:1:236. doi:10.1016/j.conb.2014.02.010

Fox C, Evans M, Pearson M, and Prescott T. 2012. Tactile SLAM with a biomimetic whiskered robot. In *IEEE International Conference on in robotics and automation (ICRA),* 4925-4930.

Gibson JJ. 1962. Observations on active touch. *Psychological Rev,* **69**: 477-491.

Gibson JM and Welker WI. 1983. Quantitative studies of stimulus coding in first-order vibrissa afferents of rats. 1. Receptive field properties and threshold distributions. *Somatosens Mot Res,* **1**:51-67. doi: 10.3109/07367228309144540

Hubel DH. 1959. Single unit activity in striate cortex of unrestrained cats. *J Physiol,***147.2**: 226-238. doi: 10.1113/jphysiol.1959.sp006238

Huber D, Gutnisky D, Peron S, O'Connor DH, Wiegert J. S., Tian L., Oertner T. G., Looger L. L., and Svoboda K. 2012. Multiple dynamic representations in the motor cortex during sensorimotor learning. *Nature,* **484:** 473-478. doi: 10.1038/nature11039

Jones LM, Depireux DA, Simons DJ and Keller A. 2004. Robust temporal coding in the trigeminal system. *Science,* **304**: 1986-1989.doi: 10.1126/science.1097779

Khatri V, Bermejo R, Brumberg JC, Keller A and Zeigler HP. 2009. Whisking in air: encoding of kinematics by trigeminal ganglion neurons in awake rats. *J Neurophysiol,* **101**: 1836-1846. doi: 10.1152/jn.90655.2008.

Kleinfeld D and Deschênes M. 2011. Neuronal basis for object location in the vibrissa scanning sensorimotor system. *Neuron,* **72**:455-468. doi: 10.1016/j.neuron.2011.10.009.

Knutsen PM, Biess A and Ahissar E. 2008.Vibrissal kinematics in 3D: tight coupling of azimuth, elevation, and torsion across different whisking modes. *Neuron,* **59**: 35-42.

Leiser SC and Moxon KA. 2007. Responses of trigeminal ganglion neurons during natural whisking behaviors in the awake rat. *Neuron,* **53**: 117-133.doi:10.1016/j.neuron.2006.10.036.

Lettvin JY, Maturana HR, McCulloch WS and Pitts WH. 1959. What the frog's eye tells the frog's brain. *Proc IRE,* **47**: 1940-1951.

Lewen GD, Bialek W, Steveninck RRDRV. Neural coding of naturalistic motion stimuli. *Network,* **12(3)**: 317:329.

Lichtenstein SH, Carvell GE, and Simons DJ. 1990. Responses of rat trigeminal ganglion neurons to movements of vibrissae in different directions. *Somatosens Mot Res,* **7**: 47-65. doi: 10.1152/jn.90511.2008

Lottem E and Azouz R. 2011. A unifying framework underlying mechanotransduction in the somatosensory system. *J Neurosci,* **31**: 8520-8532. doi: 10.1523/JNEUROSCI.6695-10.2011.

Mante V, Bonin V and Carandini M. Functional mechanisms shaping lateral geniculate responses to artificial and natural stimuli. *Neuron,* **58**: 625-638. doi: 10.1016/j.neuron.2008.03.011

Nelder JA and Wedderburn RWM. 1972. Generalized linear models. *J R Statist SocSer A*, **135**: 370–384.

O'Connor DH, Clack NG, Huber D, Komiyama T, Myers EW and Svoboda K. 2010a. Vibrissa-based object localization in head-fixed mice. *J Neurosci,* **30**: 1947-1967. doi: 10.1523/JNEUROSCI.3762-09.2010.

O'Connor DH, Peron SP, Huber D and Svoboda K. 2010b. Neural activity in barrel cortex underlying vibrissa-based object localization in mice. *Neuron*, **67**: 1048-1061. doi: http://dx.doi.org/10.1016/j.neuron.2010.08.026.

Pammer L, O'Connor DH, Hires SA, Clack NG, Huber D, Myers EW and Svoboda K. 2013. The mechanical variables underlying object localization along the axis of the whisker. *J Neurosci*, **33**: 6726-6741. doi:10.1523/JNEUROSCI.4316-12.2013.

Paninski L, Pillow J and Lewi J. 2007. Statistical models for neural encoding, decoding, and optimal stimulus design. *Prog Brain Res*, **165**: 493-507.doi:10.1016/S0079-6123(06)65031-0

Panzeri S, Petersen RS, Schultz SR, Lebedev M and Diamond ME. 2001. The role of spike timing in the coding of stimulus location in rat somatosensory cortex. *Neuron*, **29(3)**, 769-777.doi: 10.1016/S0896-6273(01)00251-3

Park IM, Meister ML, Huk AC and Pillow JW. 2014. Encoding and decoding in parietal cortex during sensorimotor decision-making. *Nat Neurosci*,**17**: 1395-1403. doi: doi:10.1038/nn.3800

Pearson MJ, Fox C, Sullivan JC, Prescott TJ, Pipe T and Mitchinson B. 2013. Simultaneous localization and mapping on a multi-degree of freedom biomimetic whiskered robot. In *IEEE International Conference on robotics and automation (ICRA)*, 586-592.doi: 10.1109/ICRA.2013.6630633

Perkon I, Košir A, Itskov PM, Tasič J and Diamond ME. 2011. Unsupervised quantification of whisking and head movement in freely moving rodents. *J Neurophysiol,* **105:** 1950-1962.doi: 10.1152/jn.00764.2010.

Peron SP, Freeman J, Iyer V, Guo C and Svoboda K. 2015.A Cellular Resolution Map of Barrel Cortex Activity during Tactile Behavior. *Neuron,* **86**: 783-799. doi: 10.1016/j.neuron.2015.03.027

Petersen RS, Panzeri S, and Diamond ME. 2001. Population coding of stimulus location in rat somatosensory cortex. *Neuron*, **32(3)**: 503-514.doi:10.1016/S0896-6273(01)00481-0

Petersen RS, Brambilla M, Bale MR, Alenda A, Panzeri S, Montemurro MA and Maravall M. 2008. Diverse and temporally precise kinetic feature selectivity in the VPm thalamic nucleus. *Neuron,* **60**: 890–903. doi: 10.1016/j.neuron.2008.09.041.

Petreanu L, Gutnisky D, Huber D, Xu N, O'Connor D, Tian L, Looger L and Svoboda K. 2012. Activity in motor-sensory projections reveals distributed coding in somatosensation. *Nature,* **489**: 299-303. doi: 10.1038/nature11321.

Phillips JR and Johnson KO. 1981. Tactile spatial resolution. III. A continuum mechanics model of skin predicting mechanoreceptor responses to bars, edges, and gratings. *J Neurophysiol*, **46**: 1204-1225.

Pillow JW, Shlens J, Paninski L, Sher A, Litke AM, Chichilnisky EJ and Simoncelli EP. 2008. Spatio-temporal correlations and visual signalling in a complete neuronal population. *Nature,* **454**: 995-999. doi: 10.1038/nature07140.

Poole K, Moroni M, and Lewin GR. 2015. Sensory mechanotransduction at membrane-matrix interfaces. *Pflügers Archiv-European J Physiol*, **467**: 121-132. doi: 10.1007/s00424-014-1563-6

Quist BW and Hartmann MJ. 2012. Mechanical signals at the base of a rat vibrissa: the effect of intrinsic vibrissa curvature and implications for tactile exploration. *J Neurophysiol*, **107**: 2298–2312. doi: 10.1152/jn.00372.2011.

Quist BW, Seghete V, Huet LA, Murphey TD, & Hartmann MJ. 2014. Modelling forces and moments at the base of a rat vibrissa during noncontact whisking and whisking against an object. *J Neurosci*, **34(30)**: 9828-9844.

Rajan K, Marre O and Tkačik G. 2013. Learning quadratic receptive fields from neural responses to natural stimuli. *Neural Comp*, **25**: 1661-1692. doi: 10.1162/NECO_a_00463.

Reinagel P. 2001. How do visual neurons respond in the real world? *Curr Opin Neurobiol*, **11(4)**: 437-442. doi:10.1016/S0959-4388(00)00231-2

Rice FL, Mance A and Munger BL. 1986. A comparative light microscopic analysis of the sensory innervation of the mystacial pad. I. Innervation of vibrissal follicle-sinus complexes. *J CompNeurol*, **252(2)**: 154-174. doi: 10.1002/cne.902520203

Simoncelli EP and Olshausen BA.2001, Natural image statistics and neural representation, *Ann Rev Neurosci*, **24**: 1193-1216. doi: 10.1146/annurev.neuro.24.1.1193.

Sofroniew NJ, Cohen JD, Lee AK, and Svoboda K. 2014. Natural whisker-guided behavior by head-fixed mice in tactile virtual reality. *J Neurosci*, **34**: 9537-9550. doi: 10.1523/JNEUROSCI.0712-14.2014.

Solomon JH and Hartmann MJZ. 2006. Biomechanics: robotic whiskers used to sense features. *Nature,* **443**: 525-525. doi: 10.1038/443525a.

Szwed M, Bagdasarian K and Ahissar E. 2003. Encoding of vibrissal active touch. *Neuron*, **40**: 621–630. doi:10.1016/S0896-6273(03)00671-8.

Szwed M, Bagdasarian K, Bluenfeld B, Barak O, Derdikman D and Ahissar E. 2006. Responses of trigeminal ganglion neurons to the radial distance of contact during active vibrissal touch. *J Neurophysiol*, **95**: 791-802. doi: 10.1152/jn.00571.2005.

Truccolo W, Eden UT, Fellows MR, Donoghue JP and Brown EN. 2005. A point process framework for relating neural spiking activity to spiking history, neural ensemble, and extrinsic covariate effects. *J Neurophysiol,* **93**: 1074–1089. doi: 10.1152/jn.00697.2004.

714 Whiteley SJ, Knutsen PM, Matthews DW and Kleinfeld D. 2015. Deflection of a vibrissa
715 leads to a gradient of strain across mechanoreceptors in a mystacial follicle. *J Neurophysiol,*
716 **66**: 67. doi: 10.1152/jn.00179.2015.

717 Woo S-H et al. 2014. Piezo2 is required for Merkel-cell mechanotransduction. *Nature,* **509**:
718 622-626. doi:10.1038/nature13251.

719 Yarbus AL. 1967. Eye movements and vision. New York: Plenum Press.

720 Yu C, Derdikman D, Haidarliu S and Ahissar E. 2006. Parallel thalamic pathways for
721 whisking and touch signals in the rat. *PLoS Biol*,**4**, e124. doi: 10.1371/journal.pbio.0040124

722 Zucker E and Welker WI. 1969. Coding of somatic sensory input by vibrissae neurons in the
723 rat's trigeminal ganglion. *Brain Res,* **12**: 138-156. doi:10.1016/0006-8993(69)90061-4

Figure 1. Electrophysiological recording from single primary whisker units in awake, head-fixed mice and simultaneous measurement of whisker kinematics/mechanics.

A. Schematic of the preparation, showing a tungsten microelectrode array implanted into the trigeminal ganglion of ahead-fixed mouse, whilst a metal pole is presented in one of a range of locations (arrows). Before the start of each trial, the pole was moved to a randomly selected, rostro-caudal location. During this time, the whiskers were out of range of the pole. At the start of the trial, the pole was rapidly raised into the whisker field, leading to whisker-pole touch. Whisker movement and whisker-pole interactions were filmed with a high-speed camera.

B and C. Kinematic (whisker angle θ) and mechanical (whisker curvature κ, moment $\vec{M}$, axial force $\vec{F}_{\mathrm{ax}}$ and lateral force $\vec{F}_{\mathrm{lat}}$) variables measured for the principal whisker in each video frame. When a whisker pushes against an object during protraction (as in panel **D**, red and cyan frames), curvature increases; when it pushes against an object during retraction (as in panels and **C**), it decreases.

D. Individual video frames during free whisking (yellow and green) and whisker-pole touch (red and cyan) with tracker solutions for the target whisker (the principal whisker for the recorded unit, panel **E**) superimposed (coloured curve segments).

E. Time series of whisker angle push angle and curvature change, together with simultaneously recorded spikes (black dots) and periods of whisker-pole contact (red bars). Coloured dots indicate times of correspondingly coloured frames in **D**.

Figure 2. Primary whisker neurons encode whisker curvature, not whisker angle, during active sensation.

A. Schematic of the Generalized Linear Model (GLM).

B. For an example unit, whisker angle (top panel), whisker curvature change (middle panel) and simultaneously recorded spike train (bottom panel, black), together with predicted spike trains for the best-fitting angle GLM (bottom panel, orange) and curvature change GLM (bottom panel, blue). Spike trains discretized using 1 ms bins and smoothed with a 100 ms boxcar filter. Prediction performance (Pearson correlation coefficient, PCC) for this unit was 0.59. Inset shows tuning curves for both GLMs, computed by convolving the relevant sensory time series (angle or curvature change) with the corresponding GLM stimulus filter to produce a time series of filter coefficients, and estimating the spiking probability as a function of filter coefficient (25 bins).

C. Analogous to panel **B.** for a second example unit. Prediction performance PCC for this unit was 0.74.

D. Prediction performance between predicted and recorded spike trains) compared for GLMs fitted with three different types of input: curvature change alone; angle alone; both curvature change and angle. Each blue/orange/green dot is the corresponding PCC for one unit: large black dots indicate median; error bars denote inter-quartile range (IQR). To test statistical significance of each unit's PCC, the GLM fitting procedure was repeated 10 times on spike trains subjected each time to a random time shift: magenta dots show these chance PCCs for the unit indicated by the magenta circle; the mean chance PCC was computed for each unit and the large gray dot shows the median across units. Black circles indicate units whose PCC was significantly different to chance (signed-rank test, Bonferroni corrected, $p<0.0025$). To

facilitate direct comparison between results for curvature change GLM and angle GLM, these are re-plotted in the inset.

E. Left. Firing rate during touch episodes compared to that during non-touch episodes for each unit, compared to corresponding predicted firing rates from each unit's curvature change GLM. **Right.** Medians across units: error bars denote IQR; * denotes differences significant at $p<0.05$ (signed-rank test).

Figure 3. Primary whisker neurons encode whisker angular acceleration during free whisking

A. Mean response of an example whisking-sensitive unit to whisking amplitude, computed during non-contact episodes (dark green, shaded area shows SEM) with regression line (black). Inset shows regression line slopes (median and IQR) for whisking sensitive (green) and non-whisking sensitive (grey) units. * indicates statistically significant rank-sum test ($p=0.05$).

B. Mean response of two example units as a function of angular acceleration. The dark brown unit is the same as that shown in A.

C. Mean response of two example units as a function of whisking phase. The dark pink unit is the same as that reported in A; the light pink unit is the same as that shown as light brown in B.

D. Excerpt of free whisking **(orange)** along with activity of an example, whisking-sensitive unit (black) and activity predicted by a GLM driven by angular acceleration (brown). The unit is the same as that shown in **A**.

E. GLM prediction accuracy (PCC) for all whisking sensitive (brown) and whisking insensitive units (grey). Bars and vertical lines denote median and IQR respectively.

Figure 4. Whisker angle and whisker curvature change are highly correlated during passive whisker deflection, but decoupled during active touch.

A. Whisker angle (**top**) and whisker curvature change (**bottom**) time series, due to passive, trapezoidal stimulation of C2 whisker in an anaesthetized mouse, estimated as mean over 10 repetitions. Note that error bars (showing SEM) are present but very small.

B. Corresponding data for low-pass filtered white noise (hereafter abbreviated to 'white noise') stimulation of the same whisker.

C. Cross-correlation between curvature change and angle during white noise stimulation, for C2 whisker.

D. Cross-correlation between angle and curvature change at zero lag, for both passive stimulation under anaesthesia and awake, active sensing (median of absolute cross-correlation for each unit; error bar denotes IQR).

E. Joint distribution of whisker angle and whisker curvature change in awake, behaving mice (1 ms sampling). Different colours denote data corresponding to different recorded units. **Inset**: Analogous plot for passive, white noise whisker deflection in an anaesthetised mouse. Different colours indicate data from different whiskers.

F. Joint distribution of angle and curvature change for an example recording from an awake behaving mouse, with samples registered during touch and non-touch distinguished by colour (1 ms sampling).

G. Touch data of **F** classified according to pole position (dot colour).

SUPPLEMENT

Figure 1-figure supplement 1. Electrophysiological recording from trigeminal primary neurons of awake, head-fixed mice.

Extracellular potential recorded from the same single unit during both anaesthetized and awake epochs. Spikes belonging to the cluster of the target unit are shown by black triangles. Inset shows overlay of all waveforms belonging to this cluster.

Video 1: Video of an awake mouse, exploring a pole with its whiskers with simultaneous electrophysiological recording of a primary whisker neuron

At the start of the video, the pole is out of range of the whiskers. Whisker tracker solution for the principal whisker of the recorded unit is overlaid in red. White dots represent spikes; orange trace shows whisker angle (scale bar = 40 ^{o}); blue trace shows whisker curvature change (scale bar = 0.05 mm^{-1}). Video was captured at 1000 frames/s and is played back at 50 frames/s. Related to Figure 1.

Figure 1- figure supplement 3. Computation of axial and lateral contact forces.

Axial (F_{ax}) and lateral (F_{lat}) force components at the whisker base were calculated, in each video frame where there were whisker-pole contacts, as follows (Pammer et al. 2013). First, the point of whisker-pole contact was located (Experimental Procedures). The direction of the force $\vec{F}$ was then calculated as the normal to the whisker tangent at the contact point (Pammer et al. 2013). Moment at the base M was calculated from the whisker curvature at

the base (Material and Methods) and then the magnitude F of $\vec{F}$ was derived from the definition of moment:

$$F = \frac{M}{rsin(\varphi)}$$

where r is the magnitude of the lever arm vector $\vec{r}$ from whisker base to contact point, and φ is the angle between $\vec{r}$ and $\vec{F}$. The components F_{ax} and F_{lat} were then found by projecting $\vec{F}$ onto the tangent and normal to the whisker at its base, respectively:

$F_{ax} = Fsin\ (\theta_{base} - \theta_{contact})$,

$F_{lat} = Fcos\ (\theta_{base} - \theta_{contact})$.

Here θ_{base} is the angle between the tangent to the whisker at its base and the horizontal; $\theta_{contact}$ is the angle between $\vec{F}$ and the horizontal.

855 **Figure 2- figure supplement 1. Effect on GLM performance of quadratic input terms,**
856 **simulated repeated trials and minimal stimulus filters**

857 **A.** Angle GLM prediction performance is robust to addition of quadratic stimulus-
858 dependence. Prediction accuracy (PCC) for standard angle GLM (same data as Figure 2C of
859 main text) in comparison to quadratic GLM (see Material and Methods). Black dots denote
860 medians, error bars IQR.

861 **B.** Single-trial GLM prediction accuracy is limited by neuronal response variability.
862 Prediction accuracy (PCC) for simulated neurons. Each simulated neuron is the best-fitting
863 GLM, based on instantaneous curvature change, for its corresponding recorded unit (see
864 Material and Methods). Prediction accuracy is quantified both using the single-trial approach
865 of the main text and using a repeated-trial method only possible by virtue of using a
866 simulation. Black dots denote medians, error bars IQR.

867 **C.** Prediction accuracy of curvature-based GLMs is accounted for by tuning to instantaneous
868 curvature change.A GLM performs a temporal filtering operation on its sensory stimulus
869 input and the sensory feature(s) which it encodes is determined by this 'stimulus filter'. The
870 stimulus filters can, in principle, be complex, but we found that the ability of a GLM to
871 predict spikes (**lower left**) from curvature change was fully explained by the simple case
872 where the action of the stimulus filter is simply to multiply the sensory input by a gain factor
873 (median 0.55, IQR 0.26-0.66; p=0.35 signed-rank test).Recorded spike train (**upper left**) and
874 curvature-predicted spike trains (**lower left**) both for a 'curvature history' GLM with a length
875 5 stimulus filter identical to Figure 2D of main text and for an 'instantaneous curvature'
876 GLM with a length 1 stimulus filter. Data for unit 2 of main text Figure 2C. Prediction
877 accuracy of the curvature history GLM compared to that of the instantaneous curvature GLM
878 for every recorded unit (**right**).

879 **D.** Tuning curves for curvature change (blue) and angle (orange) of unit 1 and unit 2 in
880 Figure 2.

881

882 **Figure 2- figure supplement 2. Moment is near-perfectly correlated with axial/lateral**
883 **contact force components during pole exploration.**

884 **A.** Two example time series for simultaneously measured whisker angle, bending moment,
885 lateral force and axial force (see Material and Methods). Red bars indicate episodes of
886 whisker-pole contact.

887 **B.** Joint distribution of bending moment and lateral force (**left**), compared to that of bending
888 moment and axial force (**right**), for the same recording shown in **A**. Moment was highly
889 linearly correlated with lateral force (median absolute correlation coefficient across units
890 0.995, IQR 0.99-1.00, median R^2 of linear fit 0.99, IQR 0.97-1.00), and highly quadratically
891 correlated with axial force (median R^2 of quadratic fit 0.94, IQR 0.85-0.98). This indicates
892 that, during our conditions of pole exploration, axial force and lateral force are both
893 redundant with moment

894 **Figure 2- figure supplement 3. Example filters for curvature-based GLMs.**

895 Stimulus filter, history filter and bias term of curvature-based GLMs for two units (**A** and **B**),
896 fitted as described in Material and Methods. Both units had negative history filters (in the 2
897 ms preceding a spike), consistent with refractoriness. The stimulus filter of unit B was
898 negative (in the 5 ms preceding a spike), indicating sensitivity to negative curvature change.
899 The stimulus filter of unit A was biphasic, but with positive integral, indicating sensitivity
900 both to positive curvature change and to positive curvature change derivative. Under our
901 stimulus conditions, dominated by slow (~100 ms) time-scale whisker-pole interactions, the

former effect was dominant; derivative-sensitivity had relatively little impact on spike prediction.

Figure 3- figure supplement 1. Whisking-sensitive units exhibit heterogeneous selectivity to angular acceleration.

For each whisker-sensitive unit, an acceleration tuning curve was estimated (Figure 3B). Tuning to positive (negative) acceleration was quantified by the slope of a regression line fitted to the positive (negative) acceleration half of the tuning curve. In general, units responded to both positive and negative accelerations but to different degrees. Statistical tests, based on regression coefficients, detailed in Material and Methods, were used to differentiate the different types of unit.

913 **Figure 4-figure supplement 1: Correlations between angle and curvature change during**
914 **passive whisker stimulation can make curvature-tuned units appear angle-tuned.**

915 The data of Figure 4 show a strong correlation between whisker angle and whisker curvature
916 during passive stimulation of the whisker. To test whether this correlation might make
917 curvature-tuned units appear angle-tuned, we used a simulation approach. This allowed us to
918 generate responses from idealised neurons whose true tuning was known, by construction, to
919 be only to curvature. We simulated responses of such neurons to the curvature change time
920 series obtained from passive white noise stimulation (**A1-2**). We then trained a GLM to
921 predict these curvature-evoked spikes using only whisker angle as input (**A3-A4**). Despite
922 being fed the 'wrong' input, this GLM was able to predict the spikes accurately (for C2
923 whisker, angle PCC was 0.90, curvature change PCC 0.94; results similar for C5; **C**). This
924 result was robust to different choices of feature tuning (**B-C**).

925 **A1.**Whisker curvature change caused by the white noise stimulus applied to C2 whisker of an
926 anaesthetized mouse (same data as main text Figure 3, repeated for clarity).

927 **A2.** Spike train evoked by a simulated curvature-tuned neuron in response to the stimulus in
928 A1 (a GLM with the position filter shown in left panel of A5).

929 **A3.**Whisker angle time series corresponding to panel A1.

930 **A4**. Target response (black) compared to predicted response from best-fitting GLMs using
931 either angle (orange) or curvature change (blue) as input.

932 **A5**. **Left**. Stimulus filter used to generate the spike train of panel A2. **Middle-Right**. Best-
933 fitting stimulus filters (normalised to unit length) for GLMs trained on the spikes of panel A2
934 and the angle time series of panel A3 or the curvature change time series of panel A1
935 respectively.

B1-5.Results analogous to A1-5 for a simulated neuron tuned to curvature velocity.

C. Quantification of the GLM predictions shown in panels A4-B4.

Figure 4-figure supplement 2. Measurement of whisker bending during passive whisker deflection.

A. Four video frames taken during trapezoidal, passive whisker stimulation with whisker tracker solutions overlaid (coloured lines).

B. Curvature change (left) and corresponding tracker solutions (right) during a 45 ms episode. Coloured dots mark the times of the example frames in panel A and shading from blue to aqua indicates curvature change. This whisker has negative intrinsic curvature. As the actuator applies force to the whisker, the whisker straightens up and the curvature increases.

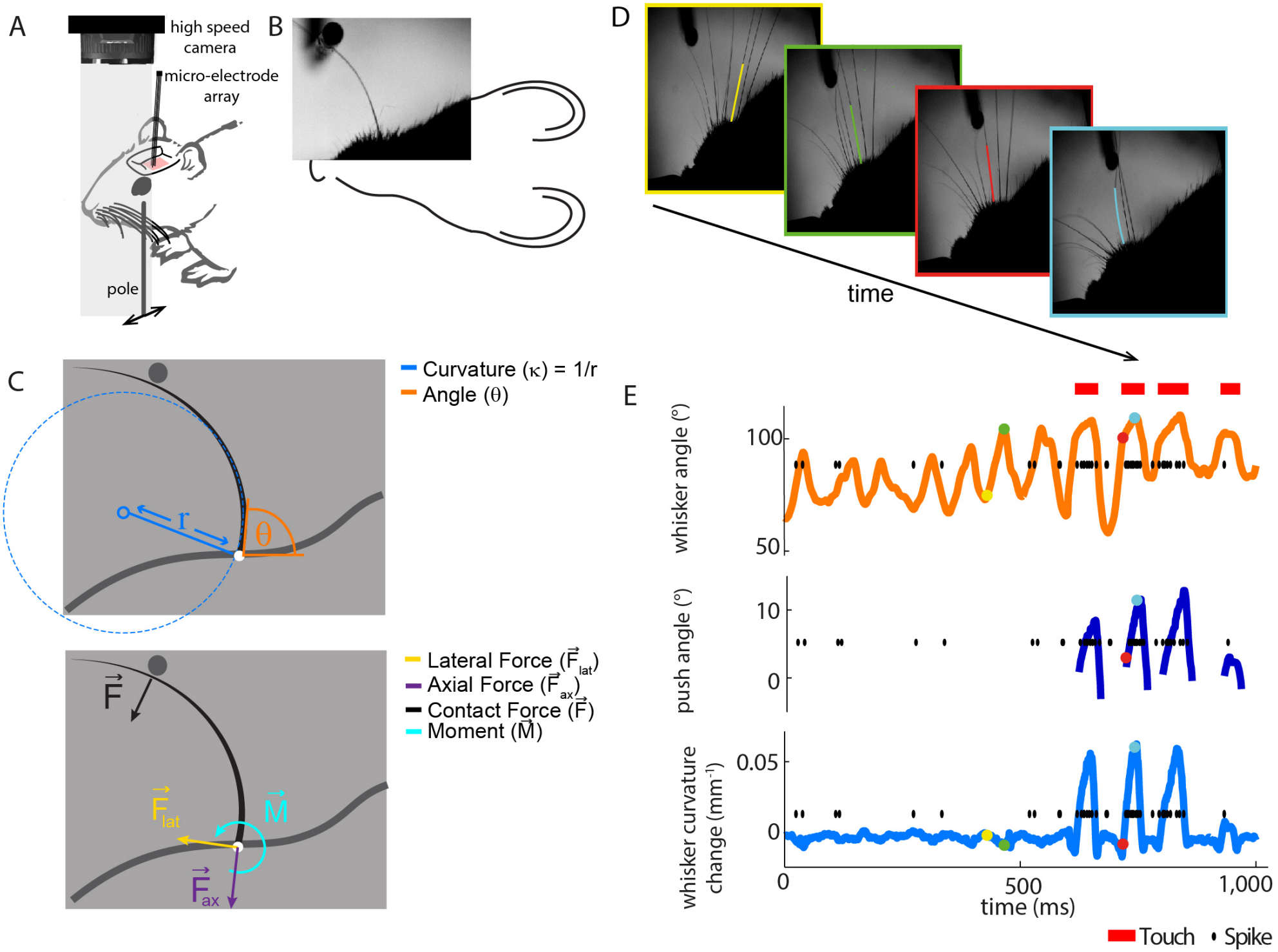
A
high speed camera
micro-electrode array
pole
B
D
time
C
Curvature (κ) = 1/r
Angle (θ)
r
θ
Lateral Force ($\vec{F}_{lat}$)
Axial Force ($\vec{F}_{ax}$)
Contact Force ($\vec{F}$)
Moment ($\vec{M}$)
$\vec{F}$
$\vec{F}_{lat}$
$\vec{M}$
$\vec{F}_{ax}$
E
whisker angle (°)
100
50
push angle (°)
10
0
whisker curvature change (mm^{-1})
0.05
0
0
500
1,000
time (ms)
Touch
Spike

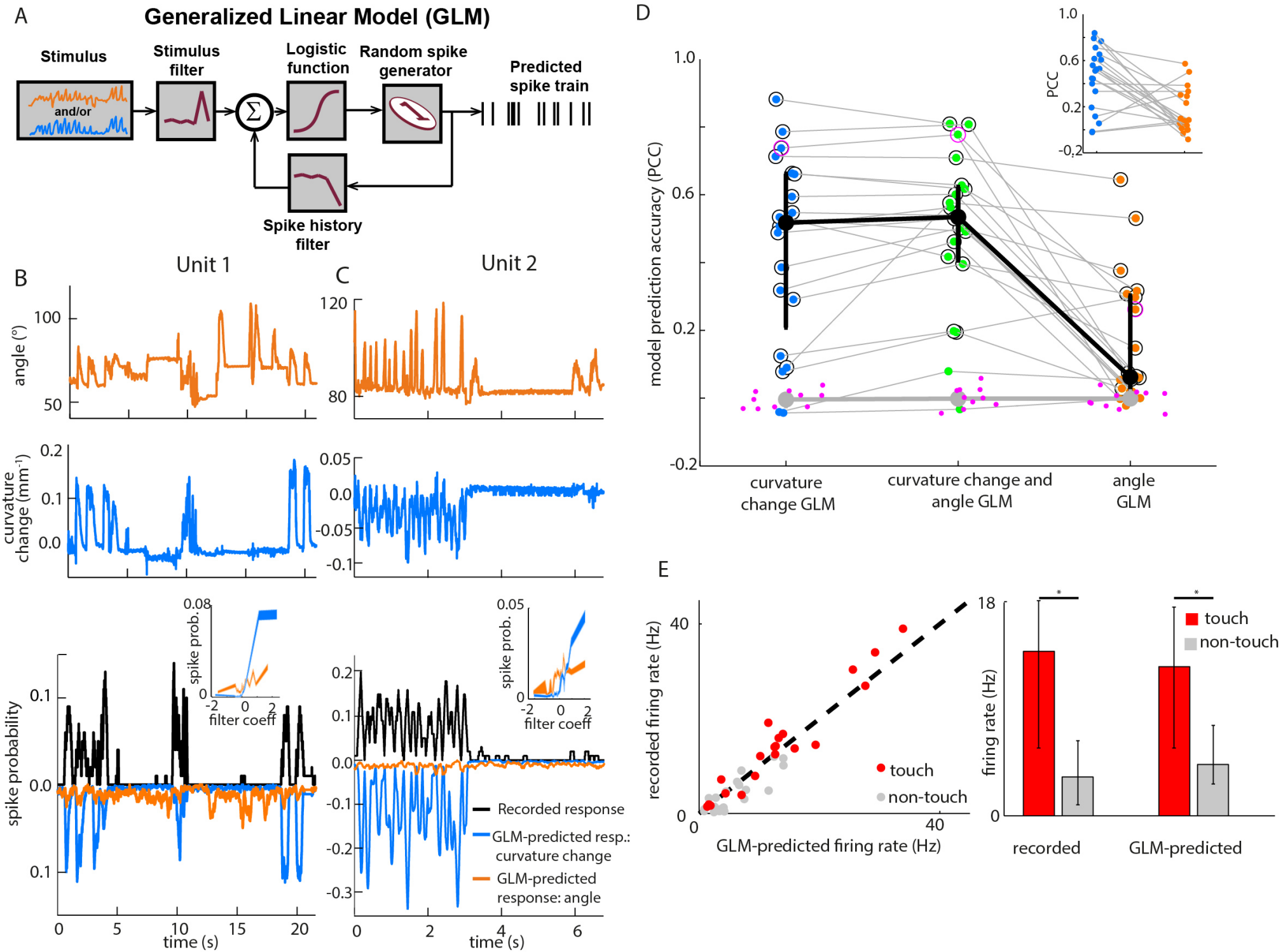
A
Generalized Linear Model (GLM)
Stimulus
and/or
Stimulus filter
Logistic function
Random spike generator
Predicted spike train
Spike history filter
B
Unit 1
C
Unit 2
angle (°)
curvature change (mm⁻¹)
spike probability
spike prob.
filter coeff
time (s)
Recorded response
GLM-predicted resp.: curvature change
GLM-predicted response: angle
D
model prediction accuracy (PCC)
PCC
curvature change GLM
curvature change and angle GLM
angle GLM
E
recorded firing rate (Hz)
GLM-predicted firing rate (Hz)
touch
non-touch
firing rate (Hz)
recorded
GLM-predicted

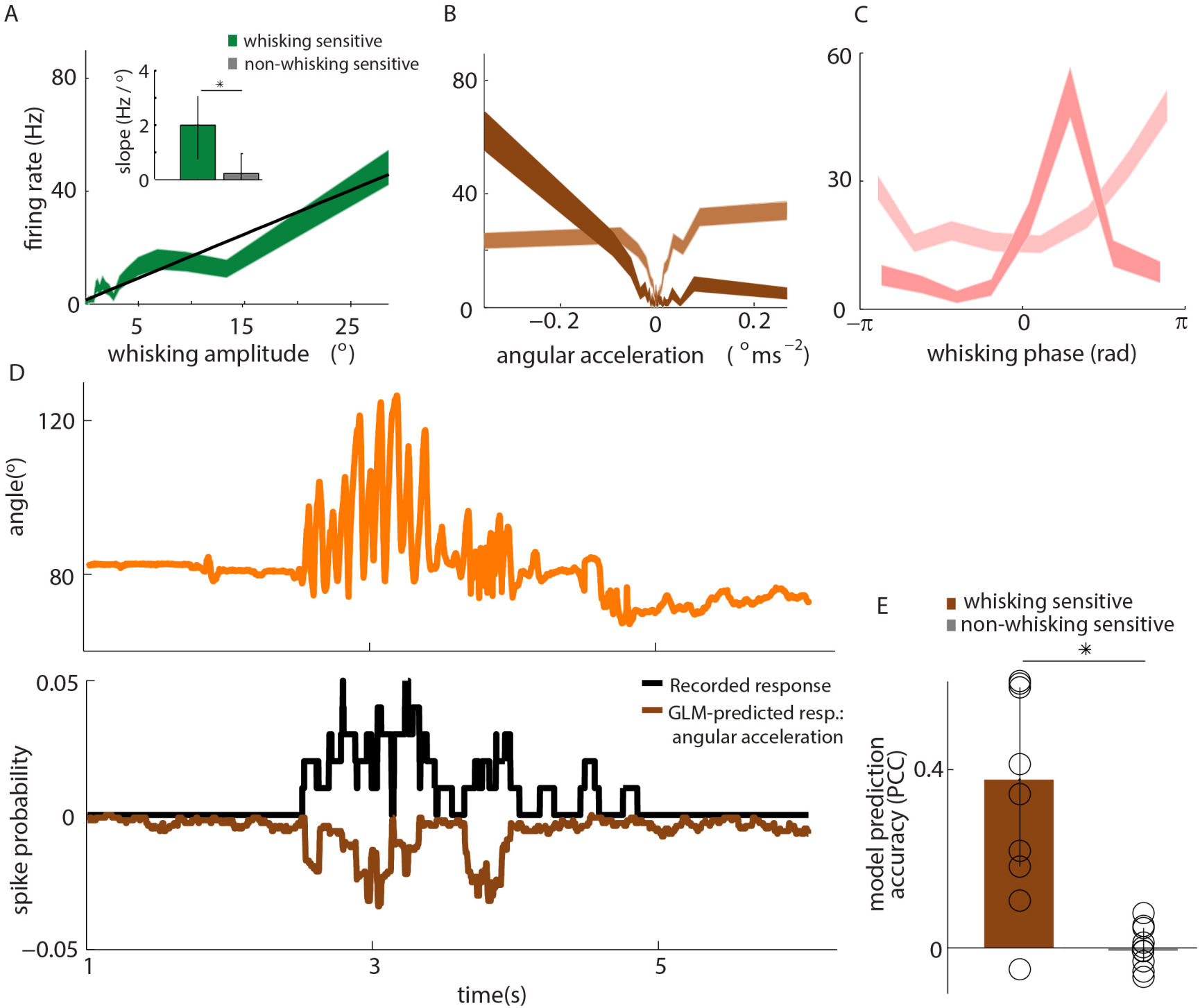
A
whisking sensitive
non-whisking sensitive
firing rate (Hz)
80
40
0
slope (Hz / °)
4
2
0
*
5
15
25
whisking amplitude (°)
B
80
40
0
−0. 2
0
0.2
angular acceleration (°ms^{-2})
C
60
30
0
−π
0
π
whisking phase (rad)
D
angle(°)
120
80
E
whisking sensitive
non-whisking sensitive
*
model prediction accuracy (PCC)
0.4
0
Recorded response
GLM-predicted resp.: angular acceleration
spike probability
0.05
0
−0.05
1
3
5
time(s)

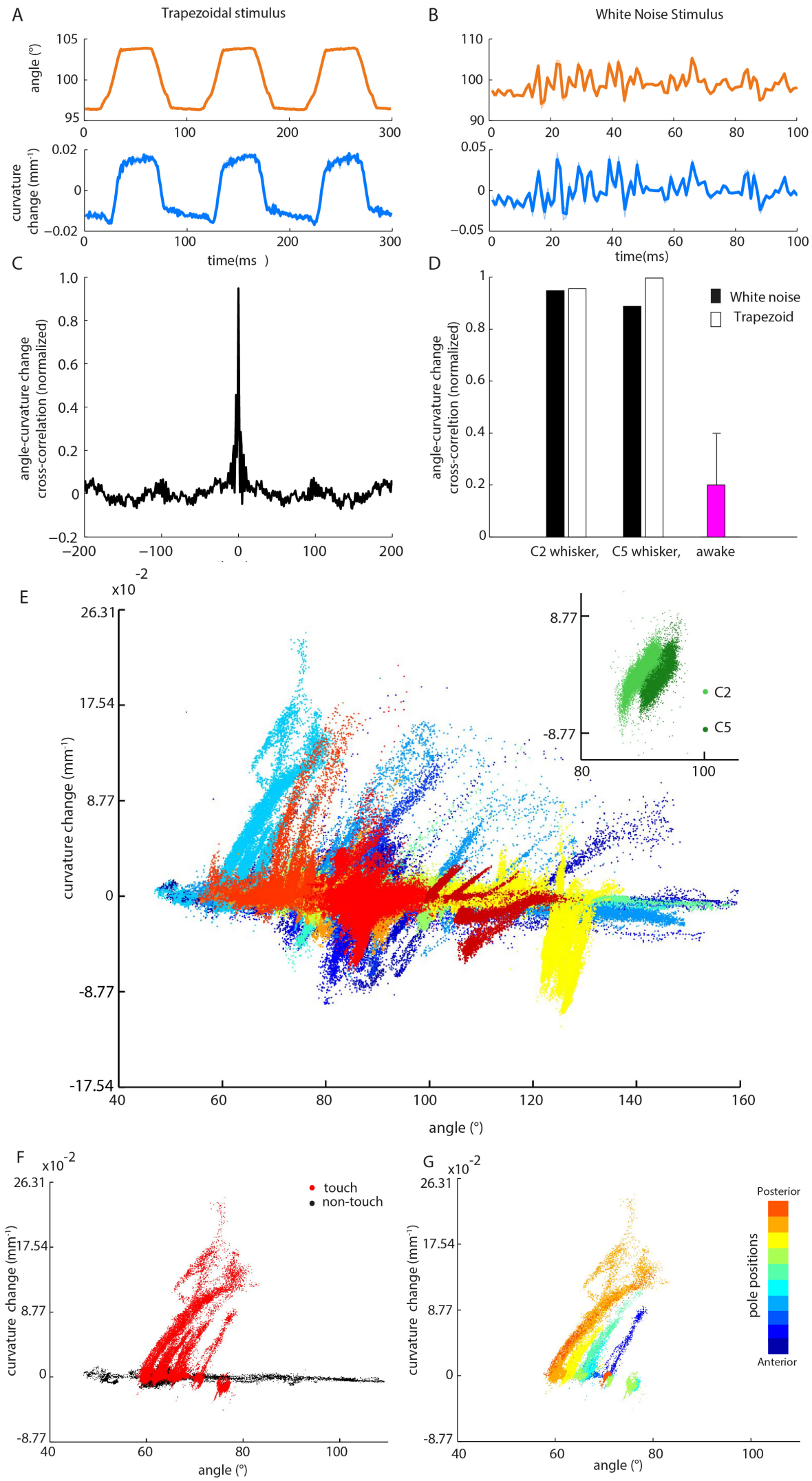
A
Trapezoidal stimulus
angle (°)
105
100
95
0
100
200
300
curvature change (mm-1)
0.02
0
−0.02
time(ms)
B
White Noise Stimulus
110
100
90
0
20
40
60
80
100
0.05
0
−0.05
time(ms)
C
angle-curvature change cross-correlation (normalized)
1.0
0.8
0.6
0.4
0.2
0
−0.2
−200
−100
0
100
200
D
angle-curvature change cross-correltion (normalized)
1
0.8
0.6
0.4
0.2
0
White noise
Trapezoid
C2 whisker,
C5 whisker,
awake
E
x10-2
26.31
17.54
8.77
0
-8.77
-17.54
curvature change (mm-1)
40
60
80
100
120
140
160
angle (°)
8.77
-8.77
80
100
C2
C5
F
x10-2
26.31
17.54
8.77
0
-8.77
curvature change (mm-1)
touch
non-touch
40
60
80
100
angle (°)
G
x10-2
26.31
17.54
8.77
0
-8.77
curvature change (mm-1)
40
60
80
100
angle (°)
Posterior
pole positions
Anterior